Article:

Genç, K., Todd, I. and Mumtaz, K. (2025) Influence of heat treatment on microstructure and magnetic properties of laser powder bed fusion generated NdFeB magnets. Progress in Additive Manufacturing, 10 (8). pp. 5743-5759. ISSN: 2363-9512

https://doi.org/10.1007/s40964-024-00941-1

Progress in Additive Manufacturing
https://doi.org/10.1007/s40964-024-00941-1

FULL RESEARCH ARTICLE

Influence of heat treatment on microstructure and magnetic properties of laser powder bed fusion generated NdFeB magnets

Kübra Genç[1] · Iain Todd[2] · Kamran Mumtaz[1]

Received: 4 June 2024 / Accepted: 19 December 2024

Abstract
Laser powder bed fusion (L-PBF) presents a promising technique for producing neodymium–iron–boron (NdFeB) magnets. However, the magnetic properties of L-PBF-generated magnets remain inferior to those of their sintered counterparts. To address this, post-processing techniques, such as heat treatment, could enhance the magnetic properties of L-PBF-fabricated NdFeB magnets. This study examines the effects of post-heat treatment on the density, magnetic properties, and microstructure of samples produced using MQP-S-11-9-20001 powder. Archimedes density measurements indicate an improvement of up to 5% in density following heat treatment, corroborated by optical images showing decreased porosity. Analysis of magnetic properties reveals an increase in remanence (B_r) alongside a decrease in coercivity (H_{ci}). Microstructural analysis indicates variations in grain size and morphology, with more distinct grain boundaries contributing to enhanced coercivity. The study also highlights challenges in analyzing high-temperature treated samples, particularly due to their extreme sensitivity to oxygen and etching difficulties. Despite these challenges, the findings offer valuable insights into how heat treatment affects the microstructure of L-PBF-generated NdFeB magnets and the resultant changes in their magnetic properties.

Keywords Laser powder bed fusion (L-PBF) · Nd–Fe–B · Permanent magnets · Heat treatment · Magnetic materials · Coercivity

1 Introduction

NdFeB magnets are one of the most common permanent magnets used in electric motors [1, 2] due to their high coercivity, H_c, high remanence, B_r, and high max energy product, BH_{max}. Eddy currents in magnetic cores during device operation generate heat, potentially raising the temperature above the Curie point of NdFeB magnets, leading to loss of magnetism and reduced performance. To mitigate this, isolated-segmented permanent magnets are used to shorten eddy current paths [3], and cooling channels are designed within motor structures. Internal cooling channels, which improve efficiency, are challenging to achieve with traditional methods but can be produced using Laser Powder Bed Fusion, L-PBF [4]. Magnet shape also impacts motor performance [5–7], though their production often relies on polymer-bonded injection molding, which compromises magnetic properties because of the polymer in them [8]. Additive manufacturing techniques such as Binder Jetting and the Fused Deposition Modelling, FDM, produce NdFeB magnets, however their magnetic properties are lower than those of sintered magnets [8–10]. The density of NdFeB magnets produced by binder jetting is significantly lower than that of sintered magnets, measuring 3.54 g/cm^3 compared to 7.5 g/cm^3 [10]. Furthermore, the remanence of binder jetting magnets (0.3 T) is inferior to that of injection molded (IM) magnets (0.5 T) and compression-bonded magnets (0.65 T) [8]. In contrast, NdFeB magnets fabricated using Big area additive manufacturing, BAAM, exhibit a slightly higher remanence (0.51 T) than IM magnets (0.48 T) but remain considerably lower than sintered magnets [11]. Similarly, FDM is not a viable additive manufacturing method for producing high-performance magnets due to its low remanence

✉ Kübra Genç
kubraa.gencc@gmail.com

Iain Todd
iain.todd@sheffield.ac.uk

Kamran Mumtaz
k.mumtaz@sheffield.ac.uk

1 Depertmant of Mechanical Engineering, University of Sheffield, Sheffield S1 4BJ, UK

2 Department of Materials Science and Engineering, University of Sheffield, Sheffield S1 4BJ, UK

Published online: 21 January 2025

(0.31 T) and density (3.57 g/cm^3) compared to IM magnets (B_r; 0.38 T, density 4.35 g/cm^3) [9]. Alternatively, sintered magnets offer superior magnetic performance but are limited by design constraints and machining challenges due to their brittle nature. Laser powder bed fusion (L-PBF) is an additive manufacturing method that uses a highly focused high power fiber laser to scan and melt metallic feedstock layer by layer to great fully dense 3D components. The process allows components to be created with a high-degree of geometric freedom within minimal material waste [10, 12, 13]. Using L-PBF to process NdFeB feedstock can facilitate the production of magnets with a higher geometric complexity compared to those conventionally manufactured (e.g. sintering), possibly expanding its applications and magnetic performance [14]. From the phase diagram of the Nd-Fe-B ternary system [15] rapid cooling leads to the formation of $Nd_2Fe_{14}B$ as the main phase alongside the precipitated B- and Nd-rich phases, and the *a*-Fe. The melt points of the B-rich, *a*-Fe, and Nd- rich phases (1081, 900 and 655 °C, respectively) are lower than the $Nd_2Fe_{14}B$ phase (1180 °C) [15]. Therefore, during cooling, the $Nd_2Fe_{14}B$ phase crystallizes earlier, at higher temperature. The Nd-rich phase crystallizes later, at lower temperature, in between the $Nd_2Fe_{14}B$ grains [16]. Laser Powder Bed Fusion (L-PBF) offers significantly faster cooling rates, which are essential for the direct crystallization of the peritectic $Nd_2Fe_{14}B$ phase [4]. In addition, L-PBF processing results in smaller grain sizes compared to sintered magnets [4] thereby enhancing coercivity [17]. The finer grains also improve the wettability of the Nd-rich phase, leading to better magnetic decoupling and further increasing coercivity [18]. However, investigations that have used L-PBF to process NdFeB have to date generated weaker magnetic properties compared to traditionally sintered magnets [19–23], this is mainly related to cracks and high levels of porosity that are created within samples [16]. Many techniques have been used to improve the magnetic properties of NdFeB magnets, they can be classified into six groups, heat treatment [24–26], infiltration [27, 28], grain boundary diffusion process [29, 30], grain refinement [17], doping [31], and intergranular addition [32–34]. This study focuses on the heat treatment influences on magnetic properties of the L-PBF processed NdFeB magnets.

Heat treatment is widely recognized for improving the magnetic properties of sintered magnets [24, 25, 36–41]. Optimizing the annealing temperature is essential for achieving significant improvements in magnetic properties. Untreated samples often exhibit a discontinuous grain boundary phase, which results in weak magnetic insulation between hard magnetic grains and low coercivity [42]. Annealing promotes the formation of a continuous Nd-rich layer between the Φ grains, effectively insulating the hard magnetic grains and suppressing exchange interactions [24, 25]. However, improper annealing temperatures, whether too high or too low, can adversely affect coercivity (H_{ci}) [37]. For instance, annealing at excessively high (> 650 °C) or low (< 550 °C) temperatures causes reversible changes in the magnetic properties [43]. Studies indicate that the optimal annealing temperature lies slightly below the melting point of the Nd-rich phase [38, 44]. However, if the temperature is significantly below the eutectic point, atomic diffusion in the solid state is limited, resulting in insufficient wetting of the 2:14:1 phase particles by the RE-rich liquid phase. This incomplete wetting fails to isolate exchange-coupled grains effectively, leading to only marginal increases in coercivity. Conversely, annealing above the melting point of the Nd-rich phase can lead to abnormal grain growth or the introduction of defects, both of which degrade coercivity [38, 41, 44].

Studies report that annealing between 500 and 620 °C increases H_{ci}, but temperatures above 680 °C cause a rapid decline [37]. Moreover, annealing at temperatures exceeding 650 °C (around the eutectic point in the Nd–Fe phase diagram) results in a gradual decrease in H_{ci}, with reductions of up to 50% observed at 800 °C [40]. Two-step heat treatments have shown even greater improvements in H_{ci}. For example, magnets annealed at 600 °C for 20 min in a high-frequency vacuum induction furnace, followed by rapid cooling in a copper mold and secondary annealing at 500 °C, achieved higher H_{ci} values (as-sintered: 1200 kA/m, single-step: 1512 kA/m, two-step: 1636 kA/m) [42]. High-frequency induction heat treatment (HIHT) also promotes the formation of a continuous Nd-rich grain boundary phase, driven by strong electromagnetic stirring, which accelerates the flow of the liquid Nd-rich phase and forms a thin, uniform layer along the grain boundaries [42]. Sequential heat treatments alternating between 500 and 1050 °C have further demonstrated that the magnetic properties of annealed as-sintered Nd–Fe–B magnets are reversible and repeatable at approximately 500 °C [41]. Notably, heat treatment has little impact on the $Nd_2Fe_{14}B$ phase, resulting in negligible changes or no alteration in the remanence (B_r) value, as indicated in Table 1.

Many studies have explored how annealing affects the magnetic properties of sintered NdFeB magnets. However, there is little research on its effects on L-PBF-processed NdFeB magnets. It has been shown that the coercivity (H_{ci}) of L-PBF processed NdFeB magnets increases from 423 to 923 kA/m after annealing, while the improvement in remanence is minimal, increasing only from 0.57 to 0.58 T [45]. In addition, findings indicate that while heat treatment cannot heal cracks in L-PBF-produced NdFeB samples, it does result in cracks with smaller diameters compared to those in as-printed samples [26]. This occurs because layers form around the open cracks after heat treatment, which appear as light-colored areas in microscope images. Energy-dispersive X-ray spectroscopy (EDX) analysis reveals a high oxygen content in these light-colored regions. The same study

Table 1 The magnetic properties of the sintered and L-PBF produced samples before and after heat treatment (The annealing temperatures listed in the table are the specific temperatures that result in the highest magnetic properties as reported in the reference papers)

	Before HT B_r (T)	After HT B_r (T)	Before HT H_{ci} (kA/m)	After HT H_{ci} (kA/m)	Heat treatment details	Ref
Sintered	1.17	1.17	1399	1560	900 °C—1 h 550 °C—1 h	[35]
Sintered	1.32	1.32	1200	1636	600 °C—20 min 500 °C—1 h	[42]
Sintered	Not reported	Not reported	Not reported	1500	925 °C—5 min 450 °C—500 °C	[36]
Sintered	No change	No change	716	946	600 °C—1 h	[39]
Sintered	1.42	1.42	439	1094	520 °C—1 h	[24]
Sintered	1.21	1.21	620	724	580 °C—4.5 h	[16]
L-PBF	0.57	0.58	423	923	600 °C—10 min 500 °C—1 h	[45]
L-PBF This study	0.61	0.69	1000	1027	680 °C—4.5 h	

concluded that energy input, calculated from process parameters, is more effective than post-heat treatment in reducing the porosity of L-PBF produced NdFeB magnets [26].

Moreover, the annealing temperature depends on the coercivity of the as printed samples;low coercivity as-printed samples need to be annealed at higher temperatures to reach their maximum coercivity, up to at 700 °C, in contrast high coercivity as printed samples need to be annealed at lower temperatures [46]. Overall, it is well-documented that heat treatment improves the coercivity of NdFeB magnets, whereas their remanence remains largely unchanged, as can be seen in Table 1.

This paper will focus on the effect of the heat treatment on sample density and magnetic properties of the L-PBF generated NdFeB magnets, including discussions of microstructural analyses.The novelty of this paper lies in its focus on the microstructural changes induced by heat treatment and their corresponding effects on the magnetic properties of L-PBF-produced NdFeB magnets, a topic that has not been extensively addressed in the existing literature. The motivation for this work extends beyond technical considerations. Economically, the production of NdFeB magnets is heavily impacted by the limited supply of neodymium (Nd), a rare-earth element that drives up production costs [47]. The environmental impact of rare-earth element extraction adds further urgency to the search for more sustainable manufacturing methods [48]. Additive manufacturing (AM), offers an opportunity to reduce material waste, which can lower the materials usage. Technologically, conventional mass-production methods such as sintering are restricted to simple magnet geometries, limiting design flexibility. In contrast, L-PBF allows for the production of magnets with complex geometries, including those with internal cooling channels [4]. Consequently, adopting AM to produce Nd-Fe-B magnets presents a significant opportunity to enhance motor performance by enabling the creation of more complex magnet geometries while conserving valuable resources. The application of the L-PBF produced NdFeB magnets in electrical machines studied in [49], and it is a promising study in terms of that L-PBF produced NdFeB samples can be used in the Permanent Magnet assisted Synchronous Reluctance motor.

This paper is structured as follows: In Sect. 2, the experimental methods are described, including material selection, sample preparation, and characterization techniques. In Sect. 3, the results are presented and analyzed, with a focus on the effects of heat treatment on the density, microstructure and magnetic properties of L-PBF-processed NdFeB magnets. Finally, in Sect. 4, the main conclusions are summarized, and potential implications for further research are discussed.

2 Materials and methods

2.1 Sample fabrication

In this study samples were produced from MQP-S-11-9-20001 powder supplied by the Magnequench Corporation (Germany). The L-PBF system used was an Aconity Lab system (Germany), which is equipped with a 1070-nm wavelength-200 W continuous wave fiber laser creating an 80-µm spot size. The system is purged within an argon gas that reduces oxygen content to 100-ppm. 10 × 10 × 10 mm samples were produced with processing parameters of 130-W laser power (*LP*), 3500-mm/s laser speed (*LS*), 20-µm layer thickness (*LT*) and 30-µm hatch distance (*HD*). The scanning strategies utilized a layer-by-layer rotation of 67° for the interlayer scan lines. The parameters were chosen among the parameters studied in previous study [20], where it was reported that the B_r reaches its maximum value by the increasing *LP* to 130 W then starts to decrease, *LS*: 3500 mm/s. These parameters were also employed in the heated bed experiments detailed in the same study [20]. Consequently, using the same parameters for the heat treatment experiments allows for a direct comparison of the effects of heat treatment and heated bed conditions on the magnetic properties.

For the subsequent heat treatment, a CarboliteGero STF160180-230SN (UK-Germany), tube furnace with a maximum temperature of 1300℃ was used. The heat treatment followed the published heat treatment for conventionally produced NdFeB magnets [25]. The samples were annealed for 4.5 h at 480, 58, 680, 780 and 880 °C, under an inert gas atmosphere. Each sample was furnace-cooled to room temperature in an argon atmosphere. In this study, the selection of the annealing temperature is based on the binary and the ternary temperature of the Nd-Fe-B phase diagrams [15], and the literature [25].

2.2 Sample characterization

Sample densities were tested using the Archimedes density test in water. Four samples were annealed for each annealing temperature. The samples for porosity and crack characterization were embedded in Bakelite followed by grinding, polishing, etching, dipped in an etching solution of 2% Nital for 5 to 60 s to reveal their grain boundaries, and then analyzed using an Nikon optical microscope and scanning electron microscope (SEM) INSPECT F50 (United States). The samples that were tested for magnetic performance were ground and polished as the presence of an oxide layer on the surface can influence results. Magnetic tests were run with a Permeameter used by Arnold Magnetic Technologies, UK. Samples were magnetized with a 100-kJ charge and a 5500 kA/m magnetic field to saturate the material before conducting the magnetic test. The *B–H* curve was then plotted using a permeameter, where the samples were clamped between holders on both sides of the sample. This arrangement ensures that the magnetic field is applied uniformly on both sides of the sample, creating a more consistent magnetic field around the material.

The working principle of the permeameter test involves applying a controlled, variable magnetic field (H) to the sample, typically by passing a current through a surrounding coil. The current is gradually varied to produce a range of magnetic field strengths, starting from zero, increasing to a maximum, and then decreasing back to zero. This process is performed in both directions to obtain the full *B–H* curve. For each value of the applied magnetic field strength (H), the corresponding magnetic flux density (B) is recorded. These data points are then plotted on a graph to generate the *B–H* curve. The curve typically illustrates how the material responds to changes in the magnetic field, showing characteristics such as magnetization (the initial rise of the *B–H* curve), saturation (where further increases in H do not significantly increase B), coercivity (the field strength required to reduce *B* to zero), and remanence (the residual magnetic flux density when *H* is reduced to zero) [50].

3 Results and discussion

3.1 Density test results

The Archimedes density test results for the samples heat-treated at 480, 580, 680, 780 °C, 880, and 980 °C indicate

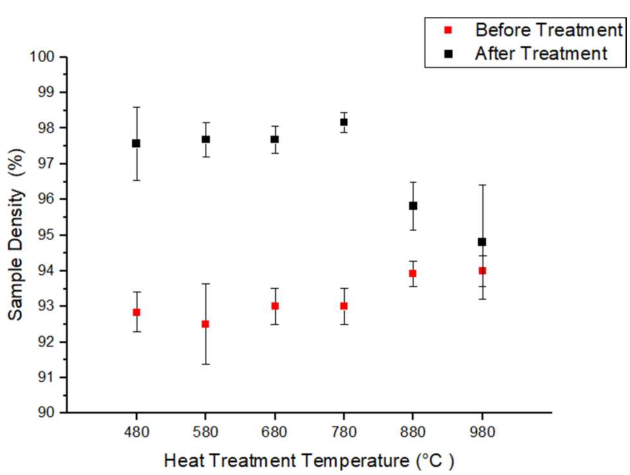

Fig. 1 Archimedes density test results in respect of heat treatment temperatures

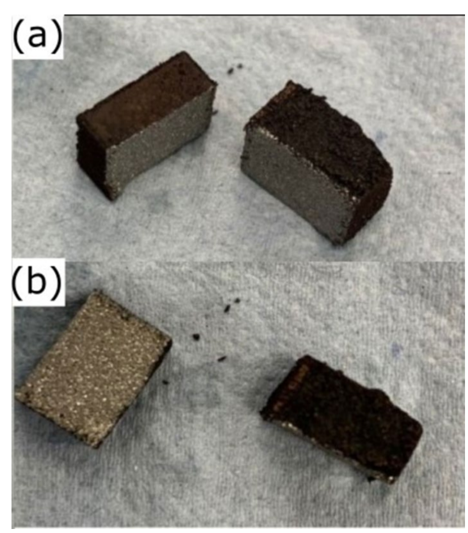

Fig. 2 Laser powder bed fusion processed NdFeB samples cut into two pieces, brown color on the sample's surfaces are oxide layers

that heat treatment can improve density by up to 5%, as shown in Fig. 1.The samples were extremely sensitive to oxidation, as evidenced by the brown oxide layer on their surfaces, with the underlying material appearing gray (Fig. 2). Optical image analysis of the samples heat-treated at 480, 780, 880, and 980 °C (Fig. 3) demonstrates improved surface quality with increased heat treatment temperature, showing fewer porosities in the samples treated at higher temperatures, the measured porosity percentages of the images are listed in Table 2. The maximum density value obtained in this study, 98%, is the highest reported in the literature for L-PBF processed NdFeB magnets, as shown in Table 3.

Despite an improvement in the sample density after heat-treatment, many cracks were observed in the cross section of the annealed samples at 580 and 680 °C, as seen in Fig. 4. These cracks are primarily oriented in the building direction, as reported in the literature, and are sensitive to oxidation [26]. It is assumed that the formation of cracks along the build direction in L-PBF processed NdFeB magnets is primarily due to the anisotropic thermal stresses caused by rapid cooling. These stresses are more intense in the build direction, where tensile forces dominate [51, 52]. The columnar grain structure that develops during solidification provides natural pathways for crack propagation [53, 54]. In addition, NdFeB's high thermal expansion coefficient and intrinsic brittleness [55] exacerbate stress concentration at grain boundaries, making them susceptible to cracking.

The existing literature indicates that the density of L-PBF processed NdFeB samples exceeds that of samples produced using polymer included additive manufacturing (AM) methods, such as BAAM, FDM, and Binder Jetting, as presented in Table 4. The density of L-PBF processed samples can be

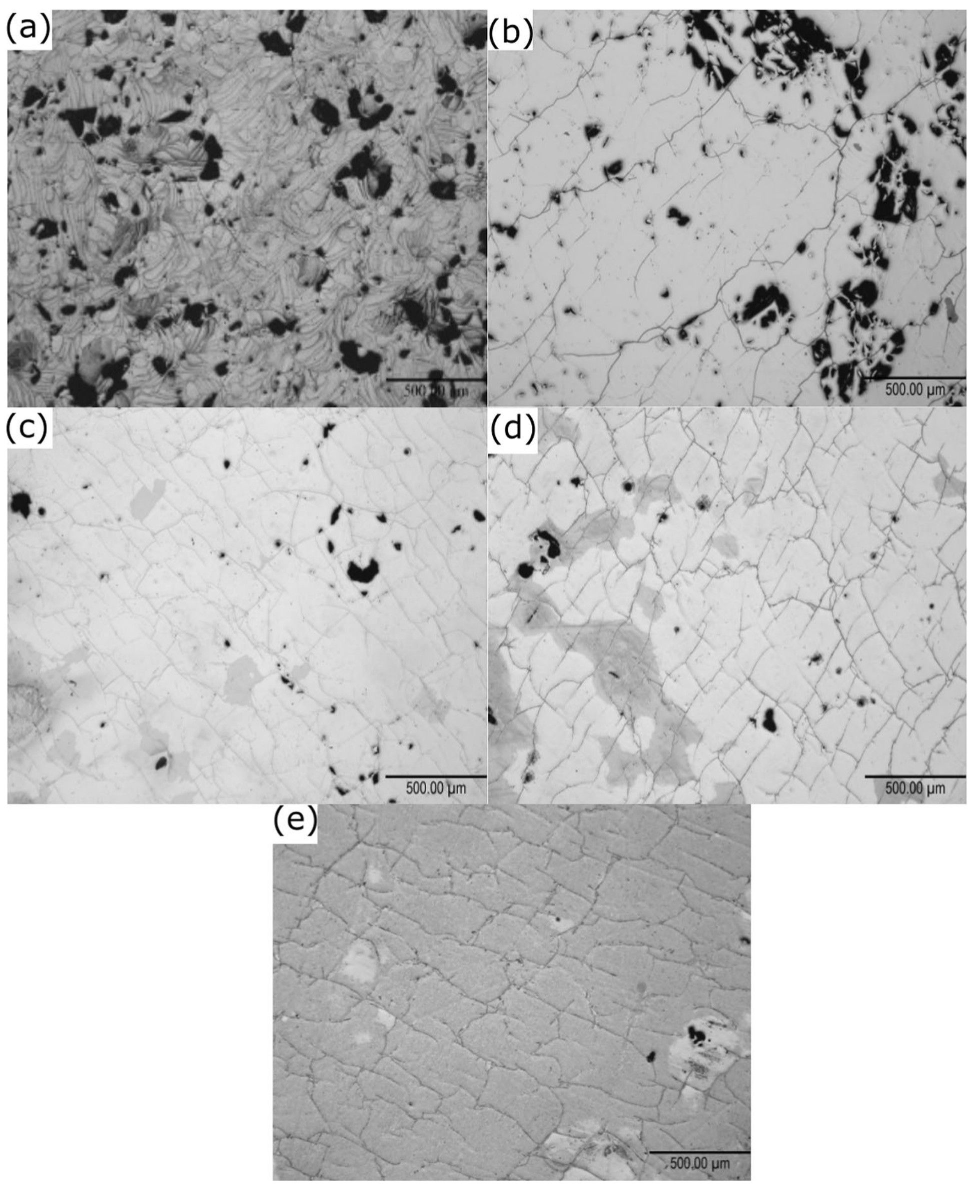

Fig. 3 Optical images of top view of the sample **a** as printed, heat treated at **b** 480 °C, **c** 780 °C, **d** 880 °C, **e** 980 °C (top view of the samples)

Table 2 Porosity Percentage of the as-printed sample and heat treated samples in Fig. 3, analysed by image J software

Heat treatment temperature	Porosity percentage, %
As-printed	9.51
480 ºC	7.82
780 ºC	1.16
880 ºC	1.10
980 ºC	0.30

improved through parameter optimization, as reported in the references in Table 3. It was found that layer thickness plays a crucial role in melt pool stability. Higher layer thicknesses result in grain coarsening due to slower cooling rates and a smaller layer thickness is required to achieve sufficient magnetic properties [22]. In addition, both magnetic polarization and sample densities decrease with increasing *LT*, from 20 to 70 µm, as reported in [56, 57]. Despite these improvements, the density of L-PBF processed magnets remains below that of sintered magnets, (sintered magnets density; 7.52 g/cm^3 [24], L-PBF processed magnet density; 7.0 g/cm^3 [4]). This limitation is attributed to the challenging brittle behavior of the alloy, which is highly sensitive to cracking caused by internal stresses [22]. In this study, the density of L-PBF processed NdFeB magnets was improved to 98% through heat treatment. This improvement is likely to enhance the remanence of the magnets, as discussed in Sect. 3.2.

3.2 Magnetic properties

Annealing plays a key role in creating a continuous Nd-rich layer between the strong magnetic phase, $Nd_2Fe_{14}B$ (known as the Φ phase), by heating the magnets above the melting point of the Nd-rich phase (655 °C) but below the melting point of the Φ phase (1180 °C) [16, 25]. These well-defined Nd-rich layers between the hard magnetic grains inhibit exchange interactions between them, thereby increasing the coercivity of the sintered NdFeB magnets without significantly affecting the B_r, as presented in Table 1. However, this study demonstrates an enhancement in B_r accompanied by a decrease in H_{ci}, as illustrated in Fig. 5. The B_r values of the printed samples improved from 0.61 to 0.69 T at 580 °C and to 0.75 T at 680 °C. However, this value begins to decline as the annealing temperature rises to 980 °C. This decline may be attributed to higher levels of oxidation in samples treated at elevated temperatures, as indicated by EDX (Energy Dispersive X Ray Analysis) measurements in Appendix 1. H_{ci} increased slightly at 580 °C, from 1000 kA/m to 1027 kA/m, then decreased to 844 kA/m at 680 °C, and continued to decrease with higher annealing temperatures, dropping to 15 kA/m at 980 °C, as depicted in Fig. 5. The H_{ci} reduction at elevated temperatures above the melting point of the Nd rich phase, 680, 780–880 and 980 °C, aligns with findings in the literature. Studies report a gradual decrease in H_{ci} starting at T > 650 °C (923 K), near the eutectic point in the Nd-Fe phase diagram [40] and after 680 °C [37]. These reductions are believed to result from annealing above the eutectic point, causing RE-rich phases to accumulate at triple junctions. This excessive phase segregation disrupts the microstructure, leading to significant degradation in coercivity [37, 40]. Moreover, it has been reported that annealing temperatures above 700 °C have a negative impact on magnetic performance. Exceeding the optimal heat treatment temperature results in a rapid decline in coercivity due to the

Table 3 Process parameters and the density values of L-PBF processed NdFeB magnets

Processing techniques	Density percentage%	Laser power, W	Laser scan speed, mm/s	Hatch distance, µm	Layer thickness, µm	Reference
L-PBF	90.9	60	160	500	60	[22]
L-PBF	86	10–100	50–1400	From 15 to 70 (in 5 µm increments)	20–30–70	[56]
L-PBF	97	40–55	1200–2000	20	20	[57]
L-PBF	Not reported	50–75–100–125–150	1000, 1500, 2000, 2500	35–75	30	[19]
L-PBF	95	55	1800	20	20	[58]
L-PBF	92	100	2250	30	20	[20]
L-PBF-heated bed	94	130	3500	30	20	[20]
L-PBF/post-heat treatment	95.71	20–60	100–150–200–300–400–500–600	20–30–40	30	[26]
L-PBF post-heat treatment	Not reported	200	2000	30	50	[45]
This study	90	130	3500	30	20	As printed
	98	130	3500	30	20	Annealing at 580 °C
	96	130	3500	30	20	Annealing at 680 °C

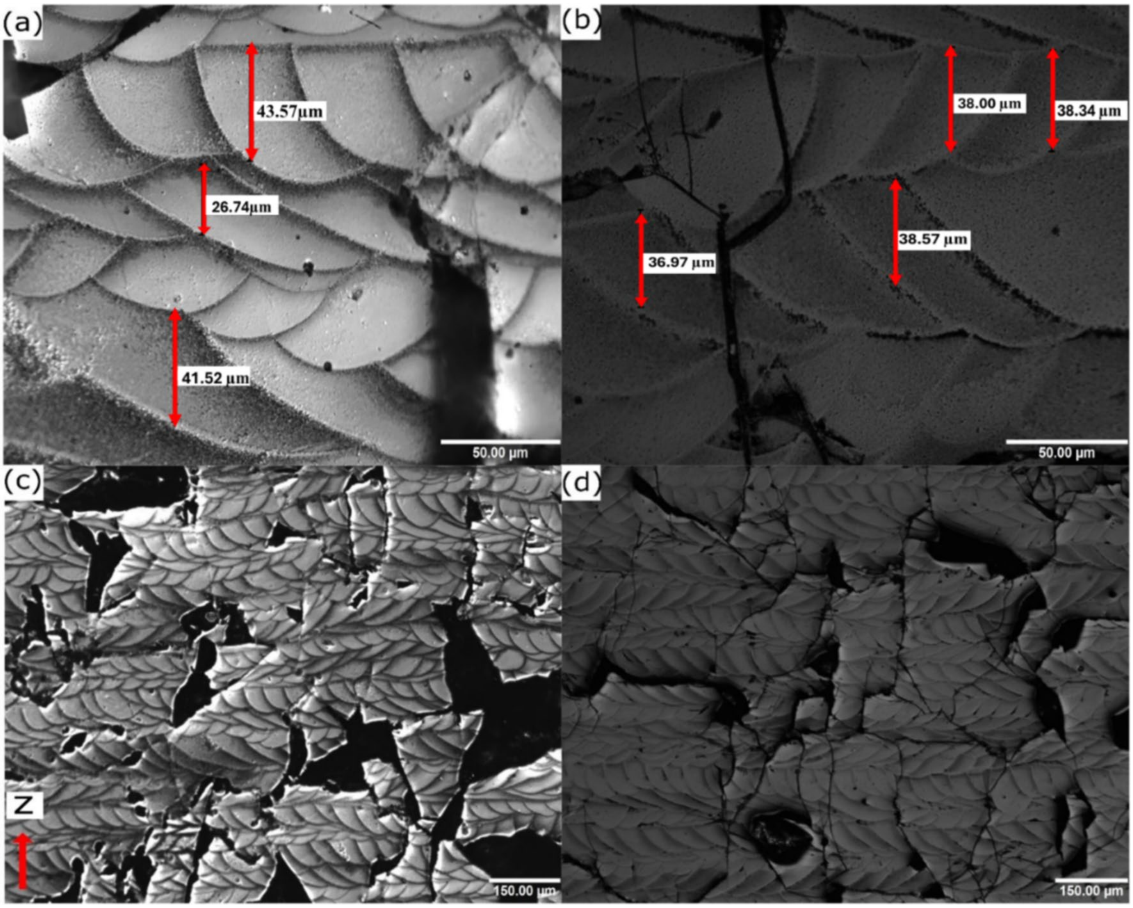

Fig. 4 The cracks across the melt pool in the build direction **a** annealed at 580 °C and **b** annealed at 680 °C

formation and growth of soft magnetic α-Fe phases within the microstructure; however, it improves the remanence of the magnets [46]. In addition, it is hypothesized that within the microscale intergranular Nd-rich regions, Fe-rich phases preferentially nucleate on the surfaces of adjacent $Nd_2Fe_{14}B$ grains. This creates surface roughness on $Nd_2Fe_{14}B$ grains, which further reduces H_{ci} [36].Therefore, in this study, the observed decrease in H_{ci} after exceeding the optimal annealing temperature may also be attributed to the increased formation of the α-Fe phase, alongside the microstructural changes discussed in the following section.

According to the literature, heat treatment does not significantly impact the density of sintered magnets (as-sintered magnet: 7.52 g/cm^3, heat-treated magnets: 7.53 and 7.54 g/cm^3) [24]. However, this study observed a notable density increase of up to 5%. Despite B_r being primarily associated with the hard magnetic phase [18], the improvement in B_r may be attributed to the enhanced sample density, as reduced porosity and cracks within the sample would mitigate magnetic loss. Coercivity is predominantly influenced by phase distribution, homogeneity, and the composition of grain boundary phases [22]. Further explanation is provided in the microstructural discussion.

Overall, in this study, magnetic properties, significantly the B_r, have improved by annealing. However, sintered NdFeB magnets are still superior to L-PBF processed NdFeB magnets, as shown in Table 4.

3.3 Microstructural evaluation

The variations in grain sizes and the grain morphology are seen in the melt pool, (as shown in Fig. 6). The solidification process of the melt pool causes variations in grain size and shape. This can be explained as follows: as the laser scans the powder on the top layer, powder melts where T > T liquidus, (in the melt pool zone) 1370 °C [4]. Due to the high scan speed of 3500 mm/s, compared to the parameters reported in the literature (see Table 3) the powder cools rapidly, resulting in the formation of fine equiaxed grains within the melt pool. They are small and in a cubic shape at the top of the melt pool, Fig. 7a, b; c oarser grains are displayed towards in the center of the melt pool, Fig. 7c, d, and finally they are coarse and equiaxed in the bottom of the melt

Table 4 Density, Remanence, B_r, and Coercivity, H_{ci}, values comparisons of additive manufacturing and conventional processing of NdFeB, adapted from [20]

Processing techniques	Density percentage%	H_{ci}, kA/m	B_r, T	$(BH)_{max}$. kJ/m^3	Reference
Binder jetting	47.2	1129	0.30	Not reported	[10]
BAAM	64	688.4	0.51	Not reported	[11]
FDM	47.6	740	0.31	Not reported	[9]
L-PBF	90.9	516	0.563	35.9	[22]
L-PBF	Not reported	923	0.58	62.3	[45]
L-PBF	92	695	0.59	45	[59]
L-PBF	86	Not reported	0.51	Not reported	[56]
L-PBF	97	Not reported	0.55	Not reported	[57]
L-PBF	91	603	0.65	62	[16]
L-PBF	Not reported	886	0.63	63	[19]
L-PBF	95	Not reported	0.56	Not reported	[58]
L-PBF	Not reported	921	0.63	63	[60]
L-PBF	92	891	0.72	81	[20]
L-PBF-heated bed	94	750	0.76	84	[20]
L-PBF/ post-heat treatment	95.71	Not reported	Not reported	Not reported	[26]
L-PBF/ post-heat treatment	Not reported	923	0.58	62.3	[45]
Sintered/post-heat treatment	Not reported	1094	1.42	381	[24]
Sintered, Arnold Magnetic Technologies	Not reported	870–2700	1–1.3	Not reported	The data were obtained from Arnold Magnetic Technologies
This study	90	1000	0.61	55	As printed
	98	1027	0.69	69	Annealing at 580 °C
	96	844	0.75	75	Annealing at 680 °C

pool as shown in Fig. 7e, f. As the laser progresses to scan the upper layer, the previously solidified layer undergoes reheating, with temperatures ranging between the liquidus (1370 °C) and solidus (1180 °C). The slower cooling rates within the heat-affected zone (HAZ) promote grain growth [61] resulting in dendritic-shaped grains aligned parallel to the build direction, as observed in Fig. 7g, h.

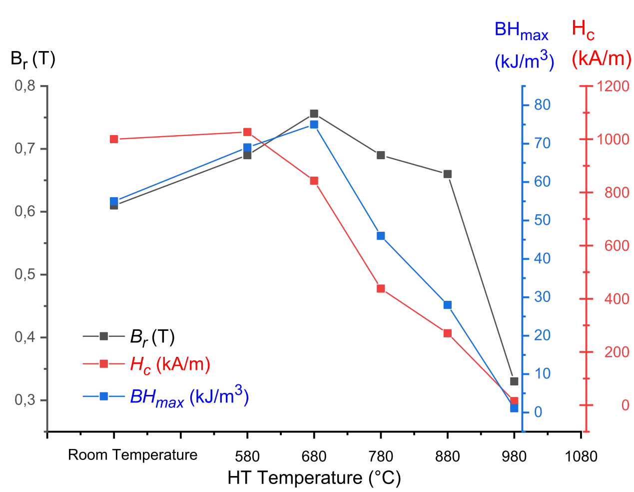

Fig. 5 Remanence, coercivity and maximum energy product of as-printed and heat-treated samples at 580, 680, 780, 880, 980 °C, tested by permeameter

The EDX findings do not reveal elemental distinctions on the sample surface, as illustrated in Fig. 8, likely due to the elements being smaller than the possible lateral resolution of the scanning electron microscope. However, the backscattering images indicate color variations within the SEM image, originating from elemental differences. A phase exhibiting brighter contrast is observed between the grains, presumed to be the RE-rich phase, while the grains themselves are assumed to be the φ phase ($Nd_2Fe_{14}B$) [45, 62]. The XRD results in this study confirm the two of the main phases $Nd_2Fe_{14}B$ phase and α-Fe phase in the samples, as seen in Fig. 9. It is know that from the phase diagram of the Nd–Fe–B ternary system in the slow cooling scenario such as sintering of NdFeB, at first is the Fe nuclei directly from the liquid phase, then Φ crystallizes at 1180 °C. These results show a high amount of α-Fe with the Φ phases in

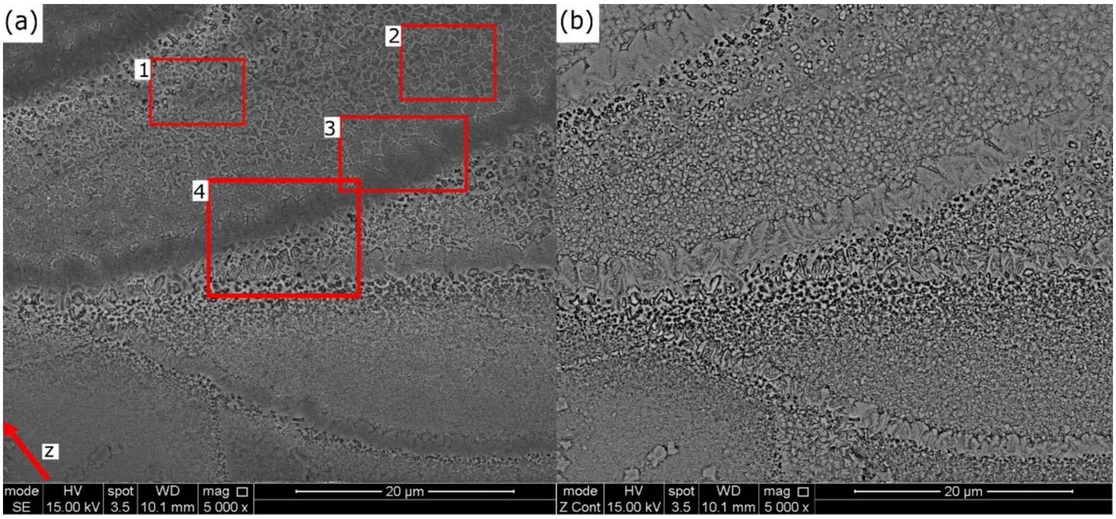

Fig. 6 Sample annealed at 580 °C, showing the grain-size distribution in the melt pool, red rectangular 1- upper side of the melt pool, 2- middle of the melt pool, 3- HAZ and the bottom of the melt pool, 4- the HAZ and the top of the melt pool below it

addition to iron boride and NdxFeyB, (they occur in very small amounts and are difficult to detect). However, the high cooling rates cause non-equilibrium cooling, which directly solidifies the Φ phase and suppresses the α-Fe phase, which still exists but at a lower amount compared to the slow cooling rate in sintered NdFeB [4], in addition to the Nd content being lower than the sintered magnets [18]. Hence, it was deduced that the light grey grains are the Φ phase with in them the black α-Fe phases and the Nd-rich phase (grey) between the grains in the back scattering images presented in Fig. 8.

The sample annealed at 680 °C exhibits variations in grain size, with smaller grains present in the narrow melt pools (see Fig. 10, square area 1) and larger grains above the HAZ, square area 2. In addition, the grain boundaries in the 680 °C sample are less continuous compared to those in the 580 °C sample (see Fig. 7). The well-defined grain boundaries at 580 °C are attributed to the high coercivity observed, whereas the discontinuous grain boundaries at 680 °C contribute to the decrease in coercivity.

The samples treated at temperatures above 680℃ were sensitive to etching. Despite diluting the etching solution and reducing the etching time, clear SEM images could not be obtained. EDX analyses revealed no elemental differences in samples treated at lower temperatures (480, 580, and 680 °C), while oxygen was predominant in samples treated at 980 °C. The EDX analysis result of the sample treated at 980 °C is provided in Appendix 1. In addition, SEM images of all samples revealed the presence of an oxide layer (white dots on the surface), as depicted in Appendix 2.

4 Conclusion

- The density of the samples increased by up to 5% following heat treatment. Despite the enhancement at the surface quality, cracks were still present in the samples, predominantly in the building direction.
- The remanence (B_r) showed a greater improvement than the intrinsic coercivity (H_{ci}), contrary to existing literature on heat-treated sintered magnets. Specifically, B_r increased from 0.61 to 0.68 T and 0.75 T with annealing at 580 and 680 °C, respectively.
- This study observed concurrent improvements in both density and B_r, suggesting a correlation between the two. Conversely, coercivity rose from 1000 to 1027 kA/m with the 580 °C treatment but dropped significantly to 15 kA/m as the temperature reached 980 °C. At 580 °C, grain boundaries were more continuous and well-defined, which is known to enhance coercivity. However, at 680 °C, these boundaries became discontinuous, resulting in a decrease in coercivity to 844 kA/m.
- The grains above the HAZ are coarse and decrease in size in the build direction as the rate of cooling is higher. In addition, it was observed that the grain morphology is differ in the melt pool, they are irregular through to the melt pool, where they are cubic just under the HAZ, and at the upper region of the melt pool.
- Analyzing the high-temperature treated samples posed significant challenges due to their extreme oxygen sensitivity and susceptibility to etching. The samples were over-etched almost immediately upon contact with etching solutions, and oxide layers formed readily on the surfaces, impairing SEM imaging and EDX analysis. Con-

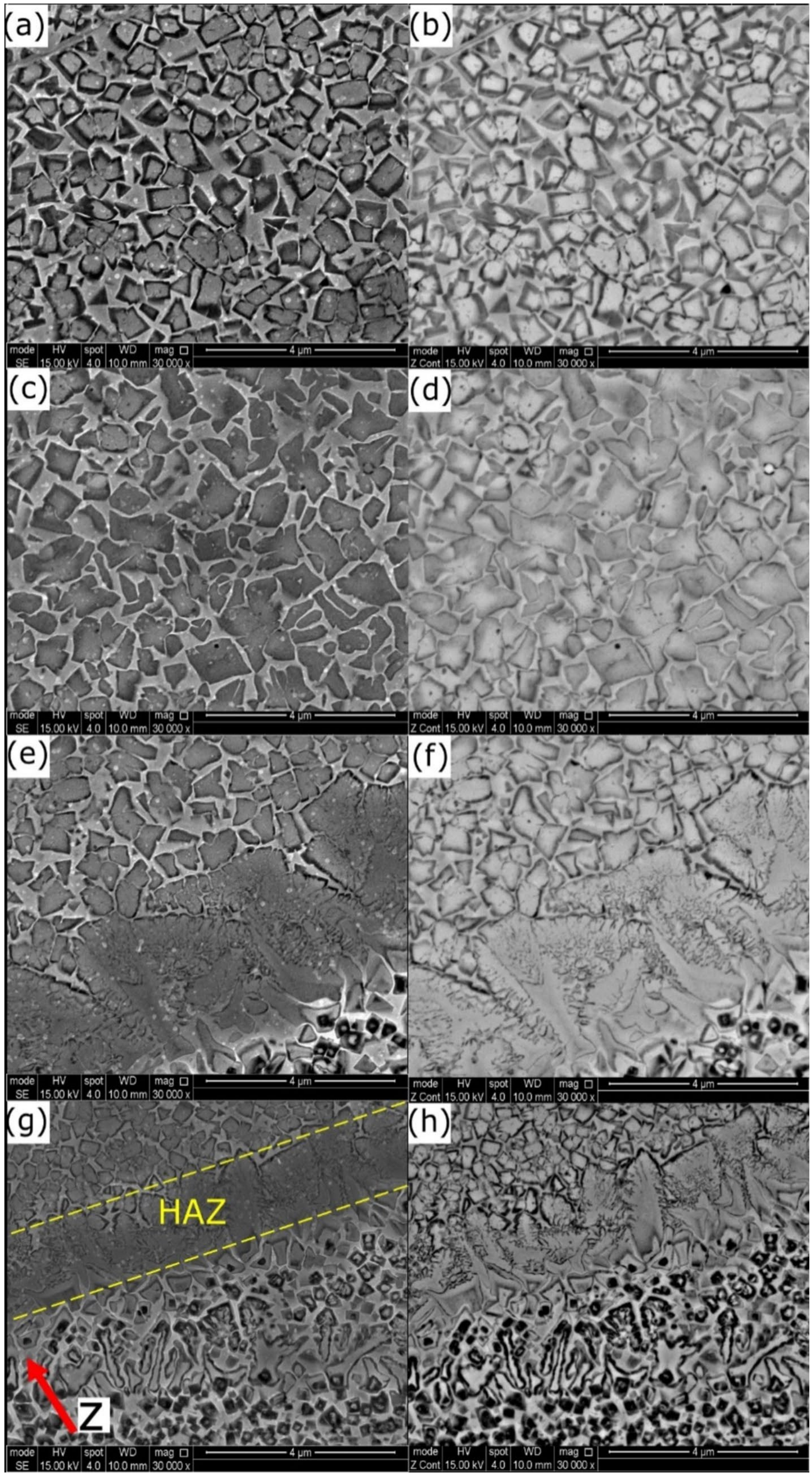

Fig. 7 Sample annealed at 580 °C **a, b** the upper side of the melt pool (cubic Φ grains with clear black a-Fe surrounding or over etched grain boundaries (could not be confirmed)) and the grey areas between grains are the Nd Rich phase, **c, d** the middle of the melt pool (equiaxed Φ grains and Nd rich phase in between them), **e, f** the bottom of the melt pool with equiaxed grains). **g, h** HAZ with the large dendritic grains in the build direction (between the yellow dot lines) and below the HAZ top of the previously melted layer with the cubic grains (lower side of the dashed lines)

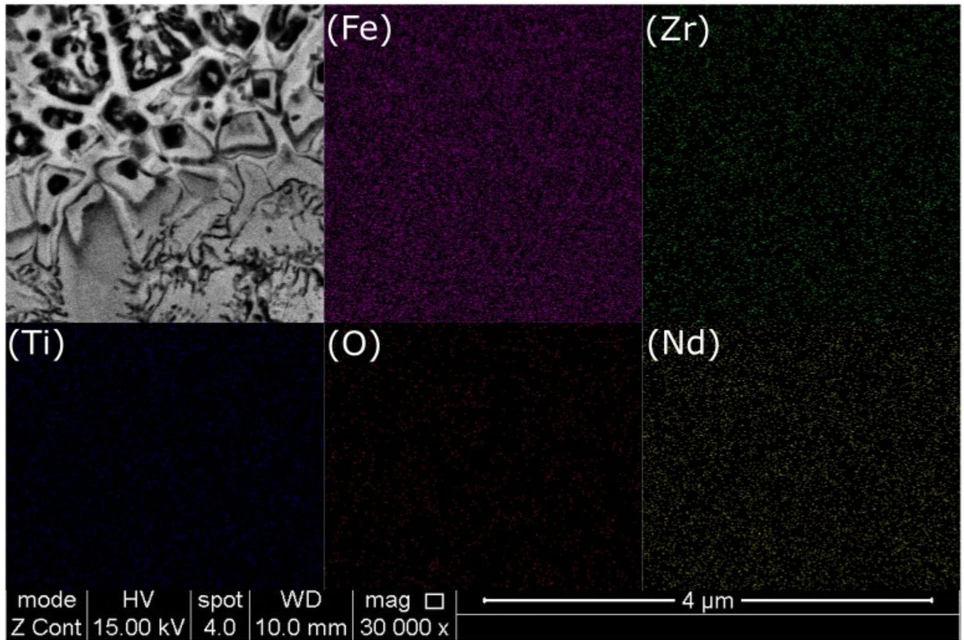

Fig. 8 EDX results of the annealed samples at 580°

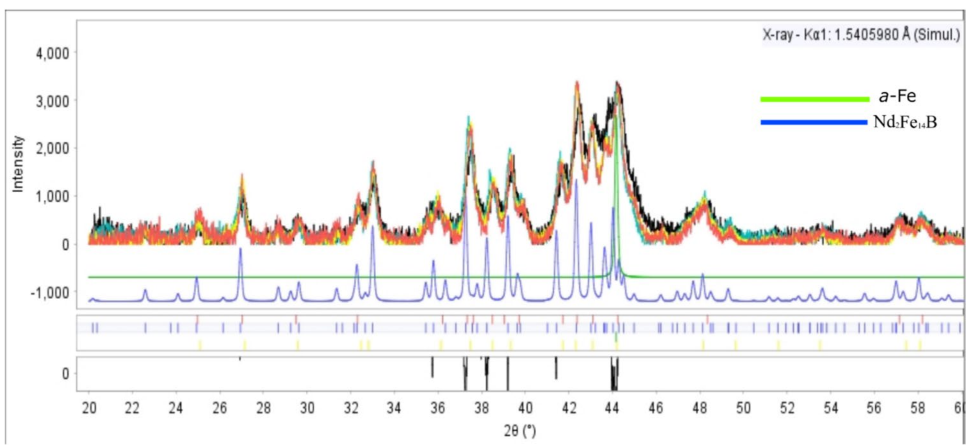

Fig. 9 XRD result of laser powder bed fusion processed NdFeB samples, after heat treatment

sequently, investigating the microstructure and elemental distribution on these sample surfaces was difficult.

The magnetic properties achieved in this study are lower than their sintered counterparts in the industry. On the other hand, heat treatment after printing has a potential to improve B_r and BH_{max} with compromising the coercivity. However, more investigations on heat treatment suggested such as quenched cooling instead furnace cooling, which might improve the microstructure hence improves both H_{ci} and B_r.

Furthermore, incorporating advanced characterization techniques to study the influence of different heat treatment processes on microstructural evolution could provide deeper insights into the relationship between processing parameters, structure, and properties. Ultimately, this research could contribute to the ongoing advancement of additive manufacturing technologies, helping to position L-PBF as a competitive method for the production of functional materials in various industrial sectors.

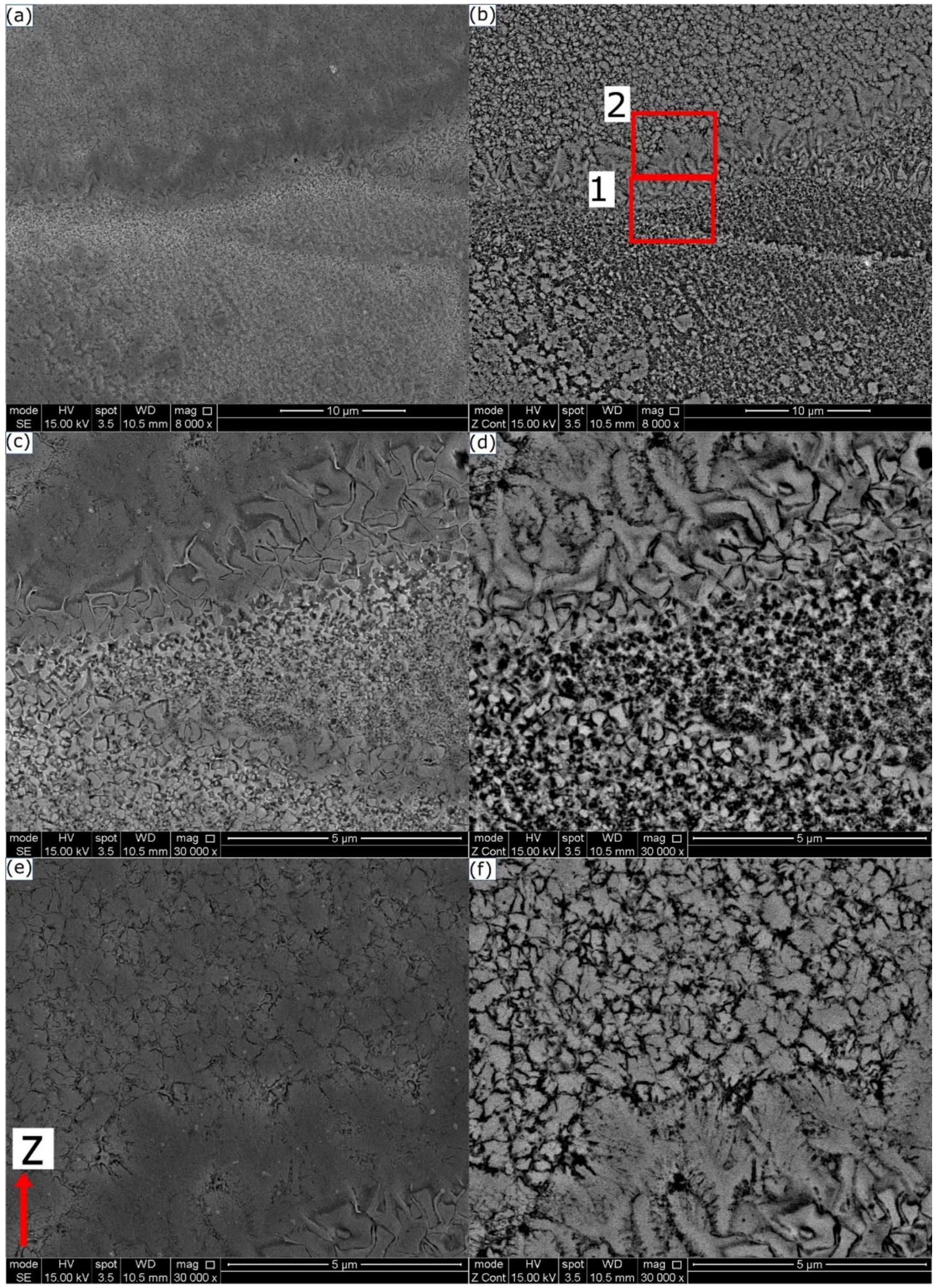

Fig. 10 SEM images of the sample annealed at 680 °C **a, b** the melt pool lines, **c, d** square box 1; narrow melt pool where the grains are finer, and **e, f** square box 2; bottom of the melt pool just above the HAZ

Appendix 1. EDX box analysis of the annealed sample at 980 °C

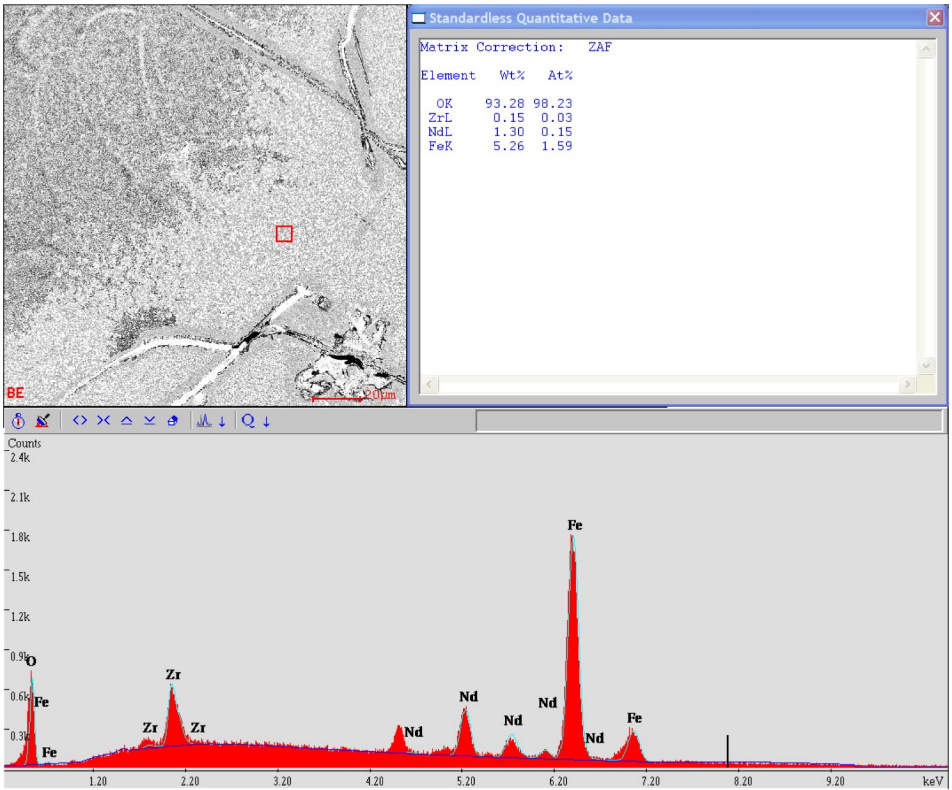

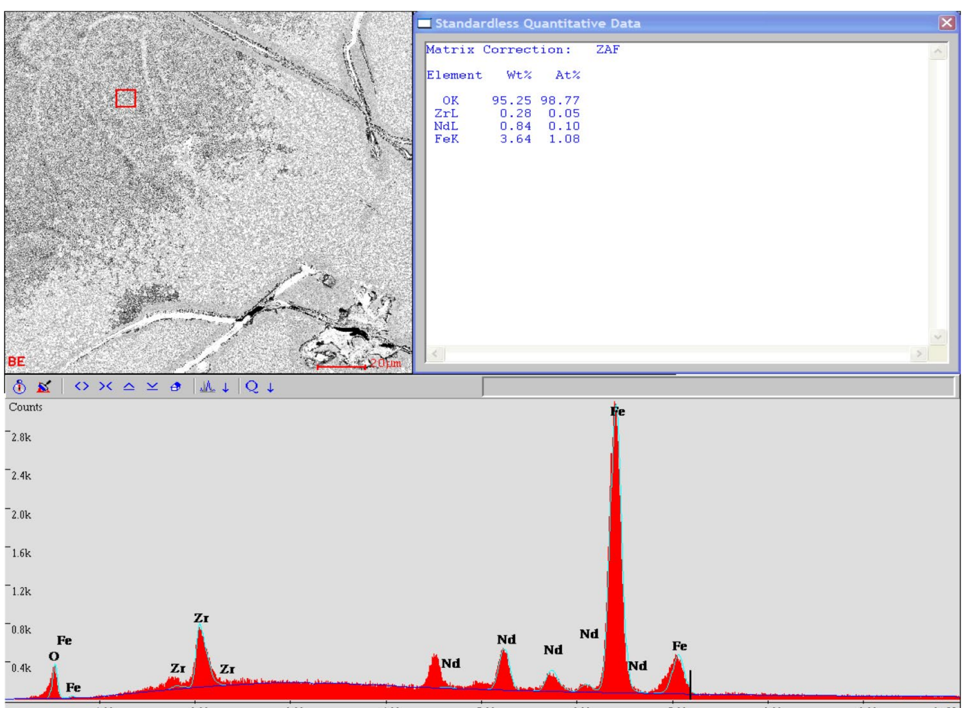

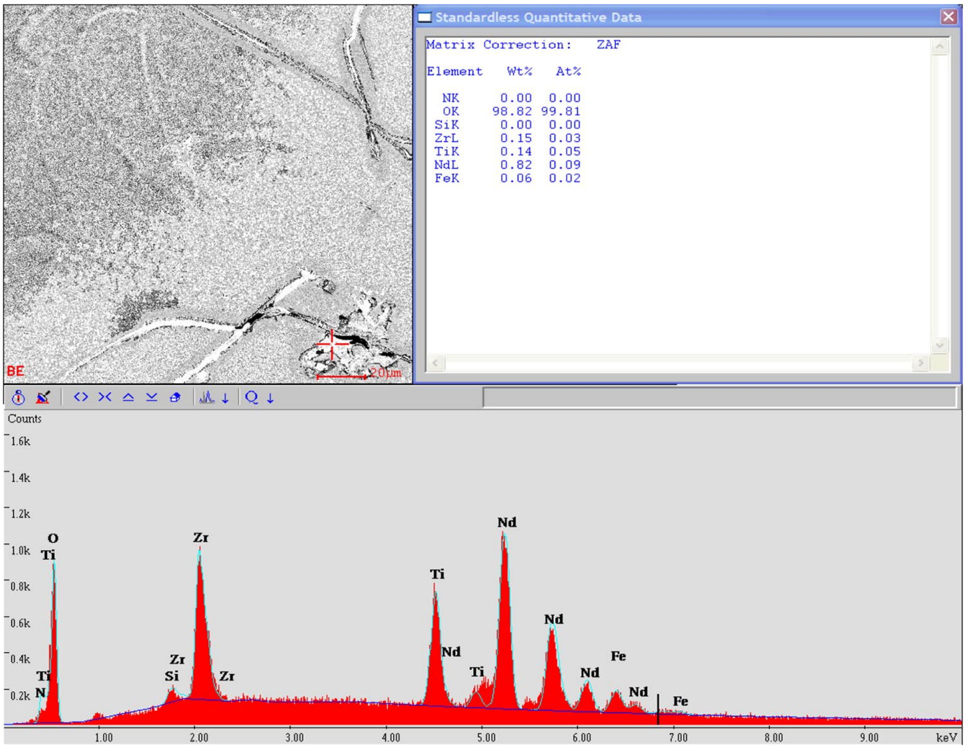

Appendix 2. SEM images of the annealed samples at 480–580–680–780–880–980 °C

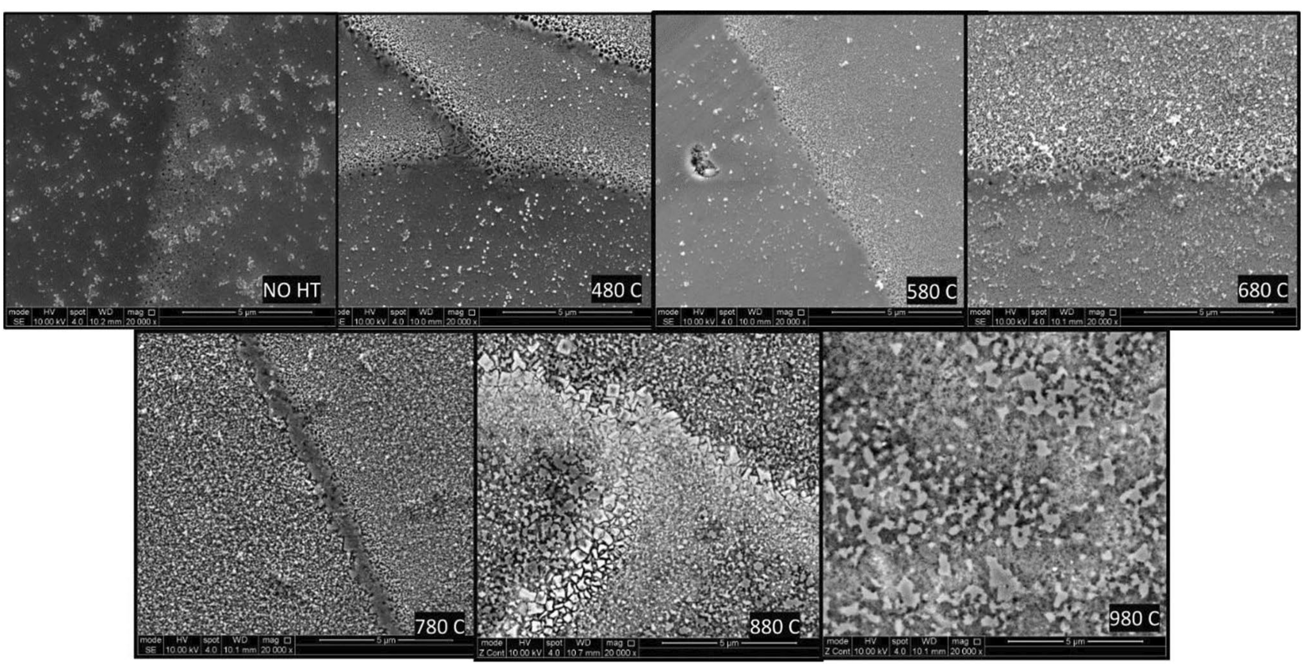

Acknowledgements The authors gratefully acknowledge Justin Mitchell and Doug Walston from Arnold Magnetic Technologies for Magnetic Tests. The authors would like to thanks the EPSRC Future Manufacturing Hub in Manufacture using Advanced Powder Processes (MAPP) (EP/P006566/1) for their support during this investigation.

Funding This study was funded by the Republic of Türkiye Ministry of National Education, HiETA Technologies Limited, and Equipmake.

Data availability The data that support the findings of this study are available from the corresponding author, Kübra Genç, upon reasonable request.

Declarations

Conflict of interest The authors declare no competing interests.

References

1. Hirosawa S, Nishino M, Miyashita S (2017) Perspectives for high-performance permanent magnets: applications, coercivity, and new materials. Adv Nat Sci Nanosci Nanotechnol 8(1):013002. https://doi.org/10.1088/2043-6254/aa597c
2. Vlachou VI *et al.*, Overview on permanent magnet motor trends and developments. Jan. 01, 2024, Multidisciplinary Digital Publishing Institute (MDPI). https://doi.org/10.3390/en17020538
3. Yamazaki K, Fukushima Y (2011) Effect of eddy-current loss reduction by magnet segmentation in synchronous motors with concentrated windings. IEEE Trans Ind Appl 47(2):779–788. https://doi.org/10.1109/TIA.2010.2103915
4. Jaćimović J et al (2017) Net shape 3D printed NdFeB permanent magnet. Adv Eng Mater 19(8):1–7. https://doi.org/10.1002/adem.201700098
5. Amin S, Madanzadeh S, Khan S, Bukhari SSH, Akhtar F, Ro JS (2022) Effect of the magnet shape on the performance of coreless axial flux permanent magnet synchronous generator. Electr Eng 104(2):959–968. https://doi.org/10.1007/s00202-021-01338-x
6. Du J, Wang X, Lv H (2016) Optimization of magnet shape based on efficiency map of IPMSM for EVs. IEEE Trans Appl Supercond 26(7):1–7. https://doi.org/10.1109/TASC.2016.2594834
7. Shokri M, Rostami N, Behjat V, Pyrhonen J, Rostami M (2015) Comparison of performance characteristics of axial-flux permanent-magnet synchronous machine with different magnet shapes. IEEE Trans Magn 51(12):1–6. https://doi.org/10.1109/TMAG.2015.2460217
8. Paranthaman MP et al (2016) Binder jetting: a novel NdFeB bonded magnet fabrication process. JOM 68(7):1978–1982. https://doi.org/10.1007/s11837-016-1883-4
9. Huber C et al (2016) 3D print of polymer bonded rare-earth magnets, and 3D magnetic field scanning with an end-user 3D printer. Appl Phys Lett 109(16):162401. https://doi.org/10.1063/1.4964856
10. Li L, Post B, Kunc V, Elliott AM, Paranthaman MP (2017) Additive manufacturing of near-net-shape bonded magnets: prospects and challenges. Scr Mater 135:100–104. https://doi.org/10.1016/j.scriptamat.2016.12.035
11. Li L et al (2016) Big area additive manufacturing of high performance bonded NdFeB magnets. Sci Rep 6:1–7. https://doi.org/10.1038/srep36212
12. Fri K et al (2023) Microstructural and heat treatment analysis of 316L elaborated by SLM additive manufacturing process. Int J Adv Manuf Technol 124(7–8):2289–2297. https://doi.org/10.1007/s00170-022-10622-4
13. Schmid S et al (2021) A new approach for automated measuring of the melt pool geometry in laser-powder bed fusion. Prog Addit Manuf 6(2):269–279. https://doi.org/10.1007/s40964-021-00173-7
14. Garibaldi M, Ashcroft I, Hague RJM, Morvan H (2015) The impact of additive manufacturing on the development of electrical machines for MEA applications: a feasibility study. [Online]. Available: https://www.researchgate.net/publication/280618833
15. Matsuura Y, Hirosawa S, Yamamoto H, Fujimura S, Sagawa M, Osamura K (1985) Phase diagram of the Nd-Fe-B ternary system. Jpn J Appl Phys 24(8A):L635–L637. https://doi.org/10.1143/JJAP.24.L635
16. Wu J, Aboulkhair NT, Degano M, Ashcroft I, Hague RJM (2021) Process-structure-property relationships in laser powder bed fusion of permanent magnetic Nd-Fe-B. Mater Des 209:109992. https://doi.org/10.1016/j.matdes.2021.109992
17. Li WF, Ohkubo T, Hono K, Sagawa M (2009) The origin of coercivity decrease in fine grained Nd-Fe-B sintered magnets. J Magn Magn Mater 321(8):1100–1105. https://doi.org/10.1016/j.jmmm.2008.10.032
18. Goll D et al (2019) Refining the microstructure of Fe-Nd-B by selective laser melting. Phys Status Solidi 13(3):1–5. https://doi.org/10.1002/pssr.201800536
19. Bittner F, Thielsch J, Drossel WG (2020) Laser powder bed fusion of Nd–Fe–B permanent magnets. Prog Addit Manuf 5(1):3–9. https://doi.org/10.1007/s40964-020-00117-7
20. Genç K, Toyting S, Galindo-Nava E, Todd I, Mumtaz K (2024) Laser powder bed fusion of NdFeB and influence of powder bed heating on density and magnetic properties. Int J Adv Manuf Technol. https://doi.org/10.1007/s00170-024-13605-9
21. Urban N, Meyer A, Kreitlein S, Leicht F, Franke J (2017) Efficient near net-shape production of high energy rare earth magnets by laser beam melting. Appl Mech Mater 871:137–144. https://doi.org/10.4028/www.scientific.net/amm.871.137
22. Skalon M et al (2019) Influence of melt-pool stability in 3D printing of NdFeB magnets on density and magnetic properties. Materials 13(1):139. https://doi.org/10.3390/ma13010139
23. Jacimovic J, Christen T, Dénervaud E (2020) Self-organized giant magnetic structures via additive manufacturing in NdFeB permanent magnets. Addit Manuf 34:101288. https://doi.org/10.1016/j.addma.2020.101288
24. Vial F, Joly F, Nevalainen E, Sagawa M, Hiraga K, Park KT (2002) Improvement of coercivity of sintered NdFeB permanent magnets by heat treatment. J Magn Magn Mater 242–245:1329–1334. https://doi.org/10.1016/S0304-8853(01)00967-2
25. Zhang Y et al (2018) Post-sinter annealing influences on coercivity of multi-main-phase Nd-Ce-Fe-B magnets. Acta Mater 146:97–105. https://doi.org/10.1016/j.actamat.2017.12.027
26. Emminghaus N, Hoff C, Hermsdorf J, Kaierle S (2020) Laser Powder Bed Fusion of NdFeB and influence of heat treatment on

microstructure and crack development. Procedia CIRP 94:211–216. https://doi.org/10.1016/j.procir.2020.09.040
27. Li L et al (2017) A novel method combining additive manufacturing and alloy infiltration for NdFeB bonded magnet fabrication. J Magn Magn Mater 438:163–167. https://doi.org/10.1016/j.jmmm.2017.04.066
28. Sato T, Oka N, Ohsuna T, Kaneko Y, Suzuki S, Shima T (2011) Enhancement of coercivity for Nd-Fe-B thin films by the infiltration of Nd-Cu alloy cap layer. J Appl Phys 110(2):1–5. https://doi.org/10.1063/1.3608244
29. Cha HR, Jeon KW, Yu JH, Kwon HW, Do Kim Y, Lee JG (2017) Coercivity enhancement of hot-deformed Nd-Fe-B magnet by grain boundary diffusion process using the reaction of NdHx and Cu nanopowders. J Alloys Compd 693:744–748. https://doi.org/10.1016/j.jallcom.2016.09.167
30. Tang M et al (2017) Microstructure modification and coercivity enhancement of Nd-Ce-Fe-B sintered magnets by grain boundary diffusing Nd-Dy-Al alloy. J Magn Magn Mater 442:338–342. https://doi.org/10.1016/j.jmmm.2017.06.116
31. Chang HW, Lee YI, Liao PH, Chang WC (2018) Significant coercivity enhancement of hot deformed NdFeB magnets by doping Ce-containing (PrNdCe)70Cu30 alloys powders. Scr Mater 146:222–225. https://doi.org/10.1016/j.scriptamat.2017.11.052
32. Cui XG et al (2017) Magnetic properties and microstructure of sintered Nd–Fe–B magnets with intergranular addition of Ni powders. J Alloys Compd 726:846–851. https://doi.org/10.1016/j.jallcom.2017.08.061
33. Zhang P, Liang L, Jin J, Zhang Y, Liu X, Yan M (2014) Magnetic properties and corrosion resistance of Nd-Fe-B magnets with Nd64Co36intergranular addition. J Alloys Compd 616:345–349. https://doi.org/10.1016/j.jallcom.2014.07.085
34. Jin C et al (2016) Magnetic properties and phase evolution of sintered Nd-Fe-B magnets with intergranular addition of Pr–Co alloy. J Alloys Compd 670:72–77. https://doi.org/10.1016/j.jallcom.2016.02.006
35. Zhou Q et al (2018) Microstructure improvement related coercivity enhancement for sintered NdFeB magnets after optimized additional heat treatment. J Rare Earths 36(4):379–384. https://doi.org/10.1016/j.jre.2017.11.007
36. Menushenkov VP, Savchenko AG (2003) Effects of post-sintering annealing on magnetic properties of Nd–Fe–B sintered magnets. J Magn Magn Mater 258–259:558–560. https://doi.org/10.1016/S0304-8853(02)01144-7
37. Liu Y, Guo S, Chen R, Lee D, Yan A (2011) Effect of heat treatment on microstructure and thermal stability of Nd-Fe-B sintered magnets. IEEE Trans Magn 47(10):3270–3272. https://doi.org/10.1109/TMAG.2011.2146239
38. Liu X, Ma T, Wang X, Yan M (2015) Coercivity enhancement of low rare earth Nd-Fe-B sintered magnets by optimizing microstructure. J Magn Magn Mater 382:26–30. https://doi.org/10.1016/j.jmmm.2015.01.043
39. Li WF, Ohkubo T, Hono K (2009) Effect of post-sinter annealing on the coercivity and microstructure of Nd-Fe-B permanent magnets. Acta Mater 57(5):1337–1346. https://doi.org/10.1016/j.actamat.2008.11.019
40. Périgo EA et al (2018) Effect of annealing conditions on the microstructure and magnetic properties of sintered Nd-Fe-B magnets as seen by magnetic small-angle neutron scattering. Mater Res Express 5(3):036110. https://doi.org/10.1088/2053-1591/aab7aa
41. Woodcock TG, Bittner F, Mix T, Müller KH, Sawatzki S, Gutfleisch O (2014) On the reversible and fully repeatable increase in coercive field of sintered Nd-Fe-B magnets following post sinter annealing. J Magn Magn Mater 360:157–164. https://doi.org/10.1016/j.jmmm.2014.02.025
42. Chen L et al (2015) Coercivity enhancement of dy-free sintered Nd-Fe-B Magnets by Grain Refinement and Induction Heat treatment. IEEE Trans Magn 51(11):1–3. https://doi.org/10.1109/TMAG.2015.2435364
43. Pathak AK et al (2016) Magnetic properties of bulk, and rapidly solidified nanostructured (Nd1-xCex)2Fe14-yCoyB ribbons. Acta Mater 103:211–216. https://doi.org/10.1016/j.actamat.2015.09.049
44. Yan M, Yu LQ, Luo W, Wang W, Zhang WY, Wen YH (2006) Change of microstructure and magnetic properties of sintered Nd-Fe-B induced by annealing. J Magn Magn Mater 301(1):1–5. https://doi.org/10.1016/j.jmmm.2005.06.003
45. Goll D, Trauter F, Bernthaler T, Schanz J, Riegel H, Schneider G (2021) Additive manufacturing of bulk nanocrystalline fendb based permanent magnets. Micromachines (Basel) 12(5):538. https://doi.org/10.3390/mi12050538
46. Bittner F, Kumar Putta A, Juerries F, Woodcock TG, Drossel WG, Thielsch J (2024) The impact of post-processing heat treatment on the magnetic properties of additively manufactured Nd-Fe-B magnets. J Magn Magn Mater 603:172238. https://doi.org/10.1016/j.jmmm.2024.172238
47. Heim JW, Vander Wal RL (2023) NdFeB permanent magnet uses, projected growth rates and Nd Plus Dy demands across end-use sectors through 2050: a review. Minerals 13(10):1274. https://doi.org/10.3390/min13101274
48. Langkau S, Erdmann M (2021) Environmental impacts of the future supply of rare earths for magnet applications. J Ind Ecol 25(4):1034–1050. https://doi.org/10.1111/jiec.13090
49. Wu J et al (2024) Additive manufacturing of Nd-Fe-B permanent magnets and their application in electrical machines. IEEE Access. https://doi.org/10.1109/ACCESS.2024.3436643
50. Franco V, Dodrill B (2021) Magnetic measurement techniques for materials characterization. Springer International Publishing, Cham
51. Lu Y et al (2015) Study on the microstructure, mechanical property and residual stress of SLM Inconel-718 alloy manufactured by differing island scanning strategy. Opt Laser Technol 75:197–206. https://doi.org/10.1016/j.optlastec.2015.07.009
52. Mercelis P, Kruth JP (2006) Residual stresses in selective laser sintering and selective laser melting. Rapid Prototyp J 12(5):254–265. https://doi.org/10.1108/13552540610707013
53. Hu YL, Lin X, Yu XB, Xu JJ, Lei M, Huang WD (2017) Effect of Ti addition on cracking and microhardness of Inconel 625 during the laser solid forming processing. J Alloys Compd 711:267–277. https://doi.org/10.1016/j.jallcom.2017.03.355
54. Wang Y et al (2022) Laser powder bed fusion of Zr-modified Al–Cu–Mg alloy: Crack-inhibiting, grain refinement, and mechanical properties. Mater Sci Eng A 838:142618. https://doi.org/10.1016/j.msea.2022.142618
55. Brown D, Ma BM, Chen Z (2002) Developments in the processing and properties of NdFeb-type permanent magnets. J Magn Magn Mater 248(3):432–440. https://doi.org/10.1016/S0304-8853(02)00334-7
56. Kolb T et al (2016) Laser Beam Melting of NdFeB for the production of rare-earth magnets. In 2016 6th International Electric

Drives Production Conference, EDPC 2016 - Proceedings, pp. 34–40, https://doi.org/10.1109/EDPC.2016.7851311
57. Urban N, Huber F, Franke J (2018) Influences of process parameters on rare earth magnets produced by laser beam melting. In 2017 7th International Electric Drives Production Conference, EDPC 2017 - Proceedings, vol. 2017, pp. 1–5, 2018, https://doi.org/10.1109/EDPC.2017.8328149
58. Urban N, Meyer A, Keller V, Franke J (2018) Contribution of additive manufacturing of rare earth material to the increase in performance and resource efficiency of permanent magnets. Appl Mech Mater 882:135–141. https://doi.org/10.4028/www.scientific.net/amm.882.135
59. Jaćimović J et al (2017) Net shape 3D printed NdFeB permanent magnet. Adv Eng Mater 19(8):1700098. https://doi.org/10.1002/adem.201700098
60. Bittner F, Thielsch J, Drossel WG (2021) Microstructure and magnetic properties of Nd-Fe-B permanent magnets produced by laser powder bed fusion. Scr Mater 201:113921. https://doi.org/10.1016/j.scriptamat.2021.113921
61. Liu X, Zhao C, Zhou X, Shen Z, Liu W (2019) Microstructure of selective laser melted AlSi10Mg alloy. Mater Des 168:107677. https://doi.org/10.1016/j.matdes.2019.107677
62. Sridharan N et al (2018) Rationalization of solidification mechanism of Nd–Fe–B magnets during laser directed-energy deposition. J Mater Sci 53(11):8619–8626. https://doi.org/10.1007/s10853-018-2178-7

Publisher's Note Springer Nature remains neutral with regard to jurisdictional claims in published maps and institutional affiliations.